Microchimica Acta (2022) 189:373
https://doi.org/10.1007/s00604-022-05474-4

ORIGINAL PAPER

Colorimetric detection of H_2O_2 with Fe_3O_4@Chi nanozyme modified µPADs using artificial intelligence

Mustafa Şen[1,2] · Elif Yüzer[2] · Vakkas Doğan[3] · İpek Avcı[2] · Kenan Ensarioğlu[4] · Ahmet Aykaç[5] · Nusret Kaya[6] · Mustafa Can[7] · Volkan Kılıç[3]

Received: 7 June 2022 / Accepted: 18 August 2022

Abstract

Peroxidase mimicking Fe_3O_4@Chitosan (Fe_3O_4@Chi) nanozyme was synthesized and used for high-sensitive enzyme-free colorimetric detection of H_2O_2. The nanozyme was characterized in comparison with Fe_3O_4 nanoparticles (NPs) using X-ray diffraction, Fourier-transform infrared spectroscopy, dynamic light scattering, and thermogravimetric analysis. The catalytic performance of Fe_3O_4@Chi nanozyme was first evaluated by UV–Vis spectroscopy using 3,3′,5,5′-tetramethylbenzidine. Unlike Fe_3O_4NPs, Fe_3O_4@Chi nanozyme exhibited an intrinsic peroxidase activity with a detection limit of 69 nM. Next, the nanozyme was applied to a microfluidic paper-based analytical device (µPAD) and colorimetric analysis was performed at varying concentrations of H_2O_2 using a machine learning-based smartphone app called "*Hi-perox Sens++*." The app with machine learning classifiers made the system user-friendly as well as more robust and adaptive against variation in illumination and camera optics. In order to train various machine learning classifiers, the images of the µPADs were taken at 30 s and 10 min by four smartphone brands under seven different illuminations. According to the results, linear discriminant analysis exhibited the highest classification accuracy (98.7%) with phone-independent repeatability at $t = 30$ s and the accuracy was preserved for 10 min. The proposed system also showed excellent selectivity in the presence of various interfering molecules and good detection performance in tap water.

Keywords Colorimetry · Smartphone detection · Hydrogen peroxide detection · Paper sensor · Android app · Machine learning · Peroxidase-like nanozyme

✉ Mustafa Şen
mustafa.sen@ikcu.edu.tr

✉ Volkan Kılıç
volkan.kilic@ikcu.edu.tr

1 Department of Biomedical Engineering, Izmir Katip Celebi University, 35620 Izmir, Turkey

2 Department of Biomedical Engineering Graduate Program, Izmir Katip Celebi University, 35620 Izmir, Turkey

3 Department of Electrical and Electronics Engineering Graduate Program, Izmir Katip Celebi University, 35620 Izmir, Turkey

4 Department of Material Science and Engineering Graduate Program, Izmir Katip Celebi University, 35620 Izmir, Turkey

5 Department of Nanoscience and Nanotechnology Graduate Program, Izmir Katip Celebi University, 35620 Izmir, Turkey

6 Department of Material Sciences and Engineering, Izmir Katip Celebi University, 35620 Izmir, Turkey

7 Department of Engineering Sciences, Izmir Katip Celebi University, 35620 Izmir, Turkey

Introduction

Hydrogen peroxide (H_2O_2) is a key molecule in a wide variety of applications, from medical diagnostics to disinfection. Peroxidase enzymes are typically used in colorimetric H_2O_2 sensor assemblies with advantages such as high catalytic activity, high substrate selectivity, wide variety of catalytic reactions, tunable activity, and excellent biocompatibility [1]. However, they suffer from some disadvantages limiting their practical applications, such as high cost, easy denaturation or protease digestion, long and difficult purification-preparation processes, and recycling [2]. Nanozymes are known as nanomaterial-based artificial enzymes that mimic the catalytic activity of enzymes [3]. In recent years, intensive efforts have been made to develop new nanozymes due to their advantages such as robust and excellent chemical stability in harsh environments, ease of production, tunable catalytic activities, flexible structure design, low cost, and good performance in controllable structure [4]. Although different analytical

Published online: 06 September 2022

methods have been used to detect H_2O_2 with nanozymes, including electrochemical, colorimetric, chemiluminescence, chromatographic, and fluorometric methods [5], colorimetric detection has attracted great attention due to simplicity, practicality, and low cost [4, 6]. The traditional approach in the colorimetric analysis is to obtain a calibration curve based on the change in absorbance or intensity in color space parameters such as RGB (Red–Green–Blue), HSV (Hue-Saturation-Value), CMYK (Cyan-Magenta-Yellow-Key) or L*a*b* (Lightness, Green–Red, Blue-Yellow) [7, 8]. While a calibration curve offers easy implementation and promising performance in a controlled environment [9, 10], it is prone to non-negligible errors and deviations due to illumination variations and camera optics under ambient light conditions, resulting in deterioration of system robustness [9]. To overcome this limitation, artificial intelligence (AI)-based approaches, such as machine learning, have emerged as useful tools for colorimetric analysis considering their flexibility and adaptability to changing conditions [11]. Machine learning can also be integrated into mobile platforms, offering quantitative and qualitative colorimetric analysis in non-laboratory and resource-limited environments [12, 13].

Herein, Fe_3O_4@Chitosan (Fe_3O_4@Chi) nanozyme was synthesized and applied to a smartphone coupled microfluidic paper-based analytical device (μPAD) for machine learning-based colorimetric analysis of H_2O_2. Due to the strong magnetic dipole–dipole attraction between particles, Fe_3O_4 nanoparticles (NPs) show a tendency to aggregate [14]. Chi has been reported to have intrinsic peroxidase activity [15]. Briefly, it can decompose H_2O_2 and form free radicals that can oxidize 3,3′,5,5′-tetramethylbenzidine (TMB) for colorimetric detection. Chi was used here both as a stabilizer to prevent NP aggregation and to increase the peroxidase activity of NPs. First, the peroxidase mimicking activity of Fe_3O_4@Chi NPs was characterized with varying concentrations of H_2O_2 using TMB and compared to those of Fe_3O_4NPs and Chi based on UV–Vis spectra. The results clearly showed that the synthesized nanozyme had high peroxidase mimicking activity for selective and sensitive detection of H_2O_2. Next, the nanozyme was applied to μPADs for machine learning-based colorimetric determination of H_2O_2. Owing to their many attractive properties, such as being low cost, practical, user-friendly, and disposable, μPADs have attracted great interest in applications ranging from environmental monitoring to bedside testing since their first introduction [16, 17]. Briefly, the Fe_3O_4@Chi nanozyme was applied to μPADs with TMB, wherein the nanozyme catalyzes TMB to ox-TMB in the presence of H_2O_2, resulting in a blue color. A machine learning-based smartphone app was developed to offer a user-friendly system as well as adaptive and robust against variation in illumination and camera optics. The features extracted from images captured with four different brands of smartphones under seven different illuminations were employed to train the machine learning classifiers. Next, the classifier with higher accuracy was integrated into the *Hi-perox Sens++* app to make the system more compact and user-friendly for end-users. In light of the results, the integrated detection platform is considered to have great potential for the colorimetric determination of H_2O_2 with fast response, simple operation, low cost, and good selectivity.

Experimental section

Materials

TMB, H_2O_2 (≥ 30 wt%), Chi – high molecular weight, acetic acid (≥ 99%), D(+)-glucose (≥ 99.5%), sucrose (≥ 99.5%), lactic acid (≥ 85%), urea (≥ 99.5%), KCl (≥ 99%), NaCl (≥ 99.5%), $CaCl_2$ (≥ 93%), $MgCl_2$ (≥ 98%), Na_2SO_4 (≥ 99%), $NaHCO_3$ (≥ 99.7%), $FeCl_2.4H_2O$ (≥ 99.0%) $FeCl_3.6H_2O$ (≥ 99.0%), NaOH (≥ 97.0%), HCl (37 wt%), and fetal bovine serum (FBS). All chemicals were supplied by Sigma-Aldrich, USA. Synthetic serum (physiologic) (Osel, Turkey). Whatman qualitative filter paper – grade 1 (Sigma-Aldrich, USA).

The synthesis and characterization of Fe_3O_4@Chi NPs

Fe_3O_4 NPs were synthesized by the co-precipitation of 1.72 g of Fe (II) and 4.7 g of Fe (III) salts in 50 mL dH_2O. Next, 3 M of ammonia was put into the iron salt solution at a speed of 10 mL h^{-1} through a syringe pump under mechanical stirring. The process was continued until the pH reached 10 and finally a black precipitate was obtained. Next, Fe_3O_4 NPs were washed with dH_2O to remove alkali metals and reach a neutral pH (pH ± 7). Samples were then freeze-dried for storage and characterization. Subsequently, Fe_3O_4@Chi NPs were synthesized. Briefly, 0.2 mg mL^{-1} of Chi solution was obtained by dissolving high molecular weight Chi in 1 M acetic acid solution. Next, 70 mg of Fe_3O_4 was added to 100 mL of Chi solution and the mixture was mixed for 18 h. Basically, Chi was adsorbed on NP surface during this process, resulting in a homogeneous dark brown suspension. The magnetic Fe_3O_4@Chi NPs were washed several times with water using a magnet. Fourier-transform infrared spectroscopy (FTIR) measurements were performed for Fe_3O_4 and Fe_3O_4@Chi NPs to verify the functional groups on their surfaces. Crystallite size, magnetic properties, morphology, and iron phase abundance of both NPs were then characterized using an X-ray diffractometer. Rietveld pattern analysis was applied to X-ray diffraction (XRD) patterns. Dynamic light scattering (DLS) was also used to measure their particle size distribution. The thermal properties of the Fe_3O_4@Chi NPs were studied using a thermogravimetric

system (TGA-SDT Q600 analyzer, TA Instruments, USA). First, 4 mg of sample was placed in an alumina crucible for analysis. Then, the temperature was raised up to 600 °C at a rate of 20 °C min^{-1}.

H_2O_2 detection using UV–Vis

TMB and H_2O_2 solutions were prepared in ethanol and dH_2O, respectively. Time-dependent absorbance of Fe_3O_4@Chi NPs was recorded every 4 s at 645 nm for 300 s in a mixture containing 50 µL of TMB, 50 µL of 2 mg mL^{-1} Fe_3O_4@Chi NPs, and 900 µL of 200 µM H_2O_2. The absorption spectrum was recorded by UV–Vis spectrophotometer in a quartz cuvette with a 1 cm path length (Evolution 201/220, Thermo Scientific, USA). Next, H_2O_2 concentration-dependent absorbance was obtained at 120 s by adding H_2O_2 at varying concentrations (0, 0.25, 0.5, 1, 10, 20, 50, 100, and 200 µM) to the mixture. For comparison, the impact of Fe_3O_4 NPs, TMB, and Chi on color change was investigated with 200 µM of H_2O_2 simply by recording the UV–Vis spectra at 120 s. Fe_3O_4 NPs and Chi were tested in the same way as Fe_3O_4@Chi NPs, where a mixture containing 50 µL TMB and 900 µL of 200 µM H_2O_2 was mixed with 50 µL 2 mg mL^{-1} Fe_3O_4 NPs and 1% (w/v) Chi in acetic acid, 2% (v/v), respectively. To investigate the impact of TMB alone on color change, 50 µL TMB was mixed with 50 µL of dH_2O and 900 µL of 200 µM H_2O_2.

Fabrication of µPADs and colorimetric detection of H_2O_2

First, a design for the µPADs was prepared using the Microsoft PowerPoint program. The design was then printed on a Whatman filter paper by a Wax printer (ColorQube 8900 Multifunction Printer, Xerox, USA). The filter paper used to produce uPADs is Whatman No. 1 filter paper. Designed in a round shape, uPADs had an inner diameter of 0.4 cm and an outer diameter of 0.6 cm. Next, the filter paper was placed on a hot plate at 120 °C for 3–4 min to facilitate the diffusion of the solid ink into the pores of the paper, thereby forming the hydrophobic barriers. Subsequently, 0.8 µL of TMB and 1 µL of Fe_3O_4@Chi NPs were added to the detection zones, respectively, and µPADs were left to dry at room temperature after each addition. Next, the µPADs were tested with H_2O_2 solutions at varying concentrations (0.01 mM, 0.05 mM, 0.1 mM, 0.2 mM, 0.5 mM, 1 mM, 5 mM, 10 mM, 25 mM, 50 mM). Briefly, 2 µL aliquots of H_2O_2 solutions were added to the detection areas of the µPADs and the color change obtained at $t = 30$ s and $t = 10$ min for each concentration level was imaged using a smartphone (Fig. 1).

Image acquisition

Image acquisition is crucial step in improving the robustness of the machine learning classifiers against adverse conditions like ambient light and camera optics [12, 13]. To operate with phone-independent repeatability under versatile illumination, a dataset for training classifiers needs to resemble all possible conditions [18, 19]. In this regard, images were captured with multiple smartphones under controlled lighting conditions, including halogen (H), fluorescent (F), and sunlight (S) bulb sources to ensure that the dataset was large enough to handle the adverse conditions. Light bulb sources, H (Osram 60 W), F (Klite 6 W), and S (Philips 5.5 W) bulbs were deliberately chosen with different characteristics as hot (2700 K), neutral (4000 K), and cold (6500 K) colors, respectively. The dataset could be enlarged using more illumination sources, but three sources were found sufficient as seven

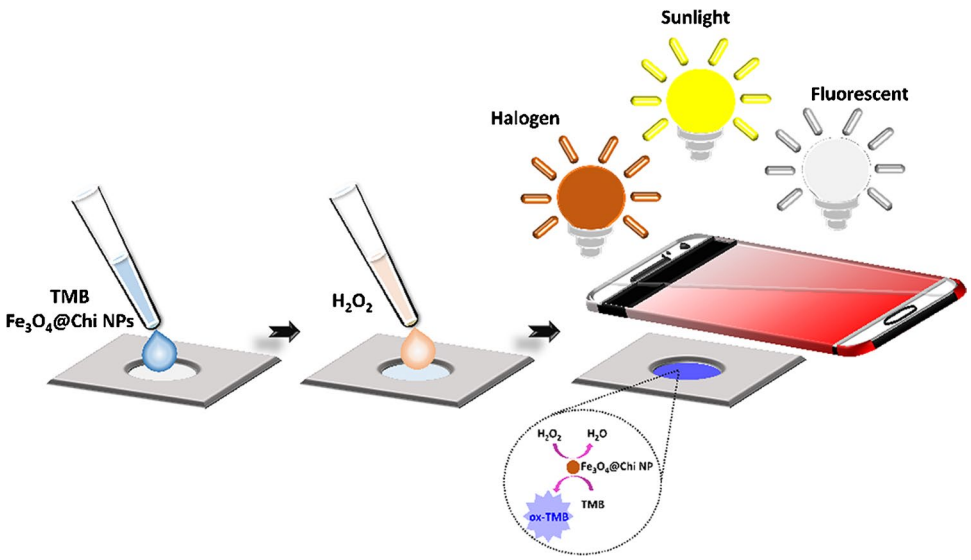

Fig. 1 A schematic representation of the system. Color change due to oxidation of TMB by Fe_3O_4@Chi NPs at varying H_2O_2 concentrations was imaged with a smartphone camera under seven different illuminations

lighting (H, F, S, HF, HS, FS, HFS) conditions were obtained using different combinations of the light sources. Images of μPADs were taken at an incident angle of 30° and a distance of 8 cm between smartphones and μPADs. In addition, the H, F, and S lamp sources were placed 50, 53, and 57 cm away from the μPADs, respectively (Fig. S1). The setup includes four different smartphones (iPhone 6S, iPhone 5SE, Oppo A5 2020 and Reeder P10) running Android and iOS with unique camera properties (Table S1) to ensure phone-independent repeatability. Smartphone cameras were used in auto mode, so that the embedded imaging software can adjust settings including shutter speed, ISO, exposure time, and color temperature. μPAD images with eight different concentration values were taken at $t = 30$ s and $t = 10$ min time intervals, resulting in 448 images for the dataset. To extract the features from these images in the MATLAB (MathWorks, MA, USA) environment, the dataset was transferred to a computer.

Feature extraction and machine learning classifiers

Feature extraction derives a new input representation with reduced dimensions containing informative and non-redundant sets of feature vectors [13]. Extracted features are crucial as classifiers learn to distinguish inputs based on these features during the training phase. Therefore, more distinctive features allow classifiers to distinguish between inputs more precisely. In this study, color and texture information are used to extract the image features, as they are promising in terms of image representation [12]. The region of interest (ROI) was cropped to convert the RGB image to HSV and L*a*b* for each concentration, so that color channels of R, G, B, H, S, V, L*, a*, b* were obtained. Then, mean, skewness, and kurtosis values of each color channel were calculated. In addition, texture properties including contrast, correlation, homogeneity, and energy were calculated. Moreover, entropy and density values were also calculated, resulting in a total of 33 features to train the classifiers in MATLAB (MathWorks, MA, USA) environment. A total of twenty-three classifiers were trained with all the extracted features to determine the H_2O_2 on μPADs. The performance comparison was evaluated in terms of classification accuracy to find the best classifier to be integrated into our *Hi-perox Sens++* app.

Smartphone application: *Hi-perox Sens++*

To test the proposed colorimetric detection of H_2O_2, our custom-designed Android application, named *Hi-perox Sens++*, was developed with improved features in terms of simplicity, speed, test options, and user-friendliness. The classification process was run on the remote server only under the MATLAB environment in the current version, leading to less computational time than the previous version, which used both MATLAB and python environments. In addition, the interface has been improved to be more straightforward and more intuitive with new screen designs and icons. The *Hi-perox Sens++* is demonstrated in Fig. 2 with screenshots. The main page of the application shown in Fig. 2a offers to capture a new photo using the smartphone camera or upload from the gallery (Fig. 2b). After the image is loaded or captured in the application, it appears on the screen (Fig. 2c). Then, the ROI is cropped using the crop box as shown in Fig. 2d to measure H_2O_2 quantitatively. The cropped ROI is displayed (Fig. 2e) to check whether the ROI is proper for analysis. If not, it can be re-cropped with the crop icon. The ROI is sent to the remote server when the upload button is tapped. The classifier on the remote server processes the ROI to classify the concentration value. Finally, the value is transferred to the *Hi-perox Sens++* from the remote server to display on the screen (Fig. 2f).

Selectivity, stability, and real sample analysis

To demonstrate the specificity of μPADs for H_2O_2, a selectivity test was performed using various interferents at 10 mM ($CaCl_2$, NaCl, KCl, $NaHCO_3$, $MgCl_2$, $CaCl_2$, Na_2SO_4, urea, sucrose, glucose, lactate solutions). After the addition of each interferent, the images of μPADs were captured at $t = 30$ s and $t = 10$ min using a smartphone camera. The images were then analyzed empirically, and the results were compared to that of 0 and 5 mM H_2O_2. In addition, a mixture containing all the interfering species was prepared at given concentrations and used for colorimetric testing of 0 and 5 mM H_2O_2. Stability test was conducted with μPADs stored at 4 °C for 0, 1, 3, 6, and 8 days. Briefly, 5 mM H_2O_2 was added to these μPADs, and the color change was imaged at 10 min under controlled lighting conditions. Water directly taken from the tap, artificial serum, and FBS were used as real samples to test the classification performance of the system. Only FBS was diluted 50 times with dH_2O. Varying concentrations of standard H_2O_2 (0, 0.05, 0.1, 0.2, 0.5, 1, 5 mM) were added into the solutions to prepare the spiked samples.

Results and discussion

Nanozyme characterization

Figure 3a shows the XRD patterns of Fe_3O_4 and Fe_3O_4@Chi NPs. Characteristic peaks were observed at 2δ of 9.6°, 30.1°,

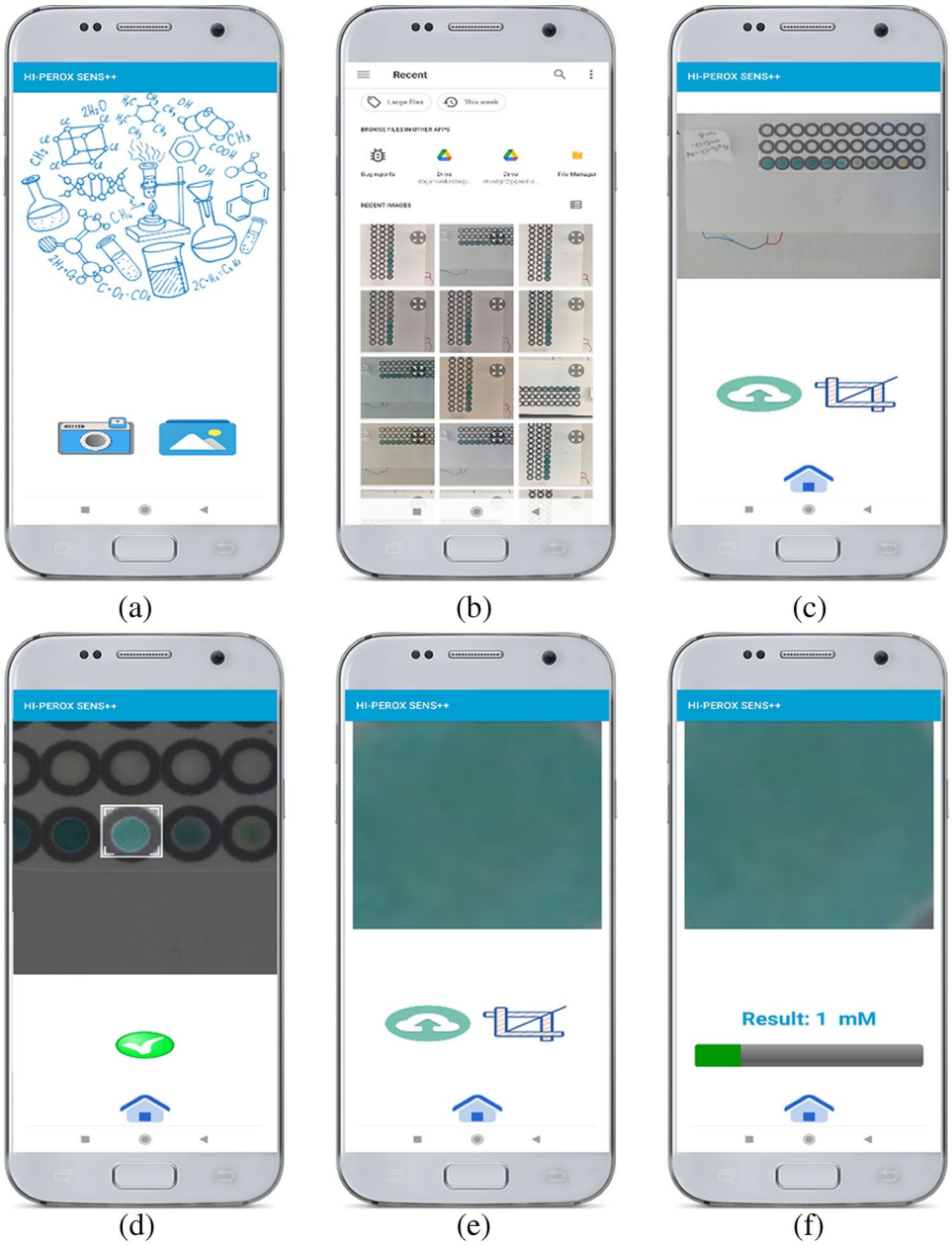

Fig. 2 Demonstration of colorimetric H_2O_2 quantification steps on the *Hi-perox Sens++*, where **a** shows the homepage. The gallery or smartphone camera can be used to select an image as shown in **b**. The selected image is displayed on the screen in **c**. An adjustable crop box is used to crop the image, and **d** shows the cropped patch. The cropped patch is uploaded in **e** to be analyzed for Fe_3O_4@Chi NPs. Finally, the result is given in **f**

35.5°, 43.1°, 54.5°, 57.6°, and 63.6° corresponding to the diffractions of 220°, 311°, 400°, 422°, 511°, and 440° crystal faces of Fe_3O_4 spinel structure (ICSD #26,410) (Fig. S2). Peak broadening indicated a small size of NPs. Modified Debye–Scherrer equation was used to assess the crystallite size of NPs from the XRD data. The broad diffraction peak of Fe_3O_4 @Chi NPs confirm that amorphous Chi polymer successfully coated the Fe_3O_4 NPs. In addition, Chi coating did not result in Fe_3O_4 NP phase change. The peaks at wavenumber of 578 and 464 cm^{-1} in FTIR spectrum of the Fe_3O_4 are considered to originate from Fe–O bands in tetrahedral and octahedral sites, confirming the Fe_3O_4 spinel type structure (Fig. 3b) [20, 21]. When compared to Fe_3O_4 NPs, the spectrum of Fe_3O_4@Chi NPs displayed a number of absorption peaks, indicating different types of functional groups present in the cross-linked beads. The broadband in the range of 3000–3600 cm^{-1} can be linked to O–H stretching vibrations and amino groups of Chi. The asymmetric and symmetric aliphatic C–H stretching bands were observed at 2931 cm^{-1}. The bands at 1625 and 1529 cm^{-1} were pertained to the C–O stretching vibration of amide and the bending vibration of $-NH_2$ groups of Chi, respectively, and 1068 cm^{-1} represented the C–O stretching vibration of C–OH of Chi [22, 23]. In addition, the strong characteristic adsorption peaks attributed to the Fe–O bond vibration of Fe_3O_4 were also observed in the IR spectrum of Fe_3O_4@Chi NPs (580 cm^{-1}) (Fig. S3),

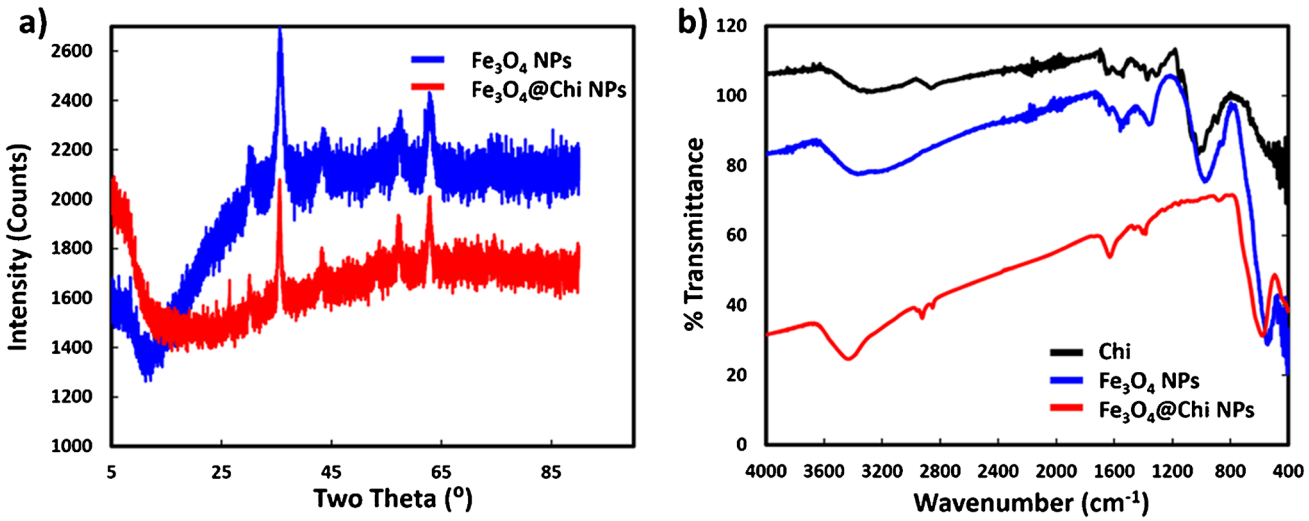

Fig. 3 XRD (**a**) and FTIR (**b**) analysis results of Fe_3O_4 and Fe_3O_4@Chi NPs

further indicating that Fe_3O_4 in Fe_3O_4@Chi NPs have been in situ formed [23]. The Chi coating of Fe_3O_4 NP was also confirmed with DLS and TGA (Fig. S4).

H_2O_2 detection via UV–Vis and μPAD

The performance of Fe_3O_4@Chi NPs for colorimetric detection of H_2O_2 was analyzed in comparison to TMB, Chi, and Fe_3O_4 NPs using UV–Vis spectroscopy. First, the time-dependent UV–Vis absorbance response of Fe_3O_4@Chi NPs at 645 nm was analyzed. As can be seen in Fig. S5a, the response attains a steady state after 100 s and for that the response at 120 s was used in the following experiments. All test groups contained the chromogenic agent TMB. As shown in Fig. 4ai and bi–ii, no color change was observed in the case of only TMB (control) and Fe_3O_4 NPs, which

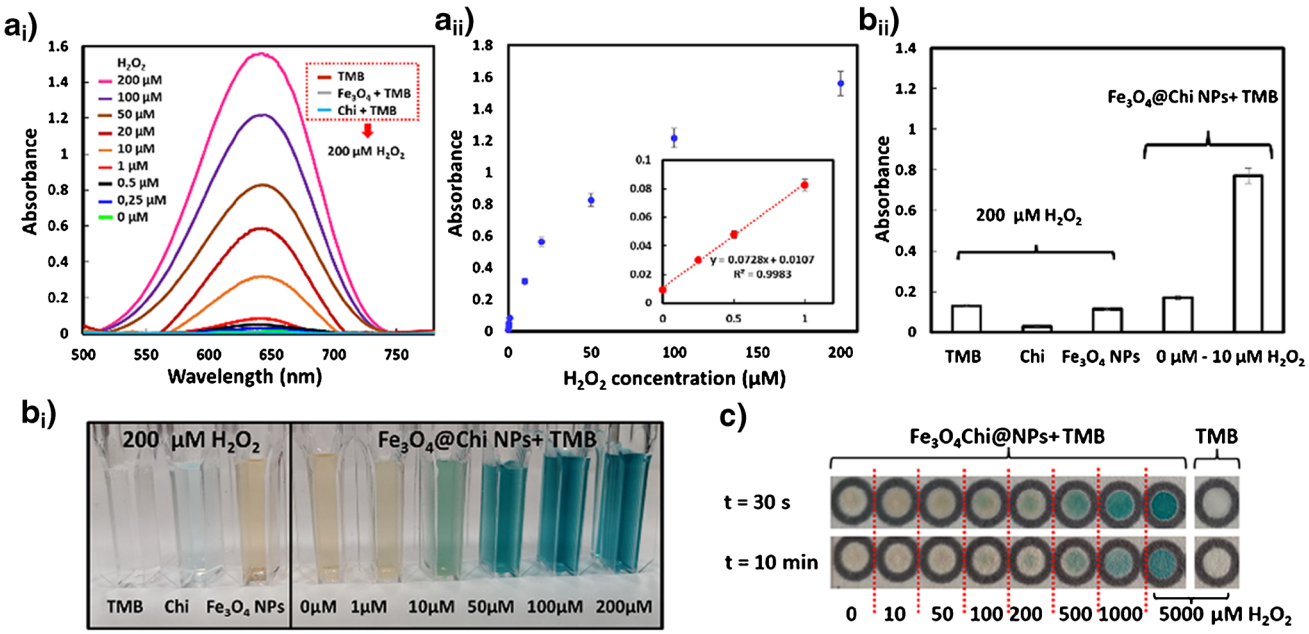

Fig. 4 UV–Vis spectra of Fe_3O_4@Chi NPs in varying concentrations of H_2O_2 along with those of TMB, Fe_3O_4, Chi in 200 μM of H_2O_2 (**a**$_i$). A calibration curve demonstrating the relationship between the response of Fe_3O_4@Chi NPs and H_2O_2 concentrations ($n = 3$) (**a**$_{ii}$). The visually observable color change (**b**$_i$), and a response comparison (**b**$_{ii}$) of TMB, Fe_3O_4, Chi, and Fe_3O_4@Chi NPs in H_2O_2 solutions at different concentrations ($n = 3$). Visually observable color changes in μPADs caused by Fe_3O_4@Chi NPs in the presence of TMB and varying concentrations of H_2O_2 compared to TMB only at 5000 μM of H_2O_2 (**c**)

clearly demonstrates that these two cannot cause any color change by themselves even in the presence of H_2O_2 at high concentration. On the other hand, Chi resulted in a blueish color, confirming its catalytic properties for the oxidation of TMB in the presence of H_2O_2 [15, 24]. However, the color change was obtained at 200 µM H_2O_2 and it was considerably lower than that of Fe_3O_4@Chi NPs at 10 µM H_2O_2. In other words, the catalytic performance of Fe_3O_4@Chi NPs was much higher than that of Chi only. Fe_3O_4@Chi NPs were then used to detect H_2O_2 at varying concentrations. Figure 4bi clearly shows that changing the H_2O_2 from 1 to 200 µM resulted in a visually observable color change. The UV–Vis absorbance data at 645 nm (Fig. 4ai) were used to obtain a calibration curve (Figs. 4aii and S5b). The limit of detection (*LOD*) of the Fe_3O_4@Chi NPs for the detection of H_2O_2 was calculated to be 69 nM ($LOD = 3 \times \sigma$/Slope). Compared to some of the recently published studies, Fe_3O_4@Chi NPs demonstrated a significantly low *LOD* with a narrow detection range (Table 1). Afterward, the Fe_3O_4@Chi NPs were applied to a µPAD as shown in Fig. 1 for the colorimetric detection of H_2O_2 using machine learning classifiers, a subset of an artificial approach. First, varying concentration of TMB (20–320 mM) was tested in µPADs to obtain the maximum color intensity. According to the results of 5 mM H_2O_2 ($t = 10$ min), increasing the concentration of TMB had no significant impact in terms of color intensity, and therefore, 20 mM of TMB (0.8 µL) was used in subsequent experiments (Fig. S6a). As for the nanozyme, it increased the color intensity as well as the background noise as it alone made the detection areas of the µPADs brown (Fig. S6b). To reduce the background noise and have much uniform color change, 1 µL aliquots of 2 mg mL^{-1} Fe_3O_4@Chi NPs were used in µPADs. Similarly, increasing the sample volume changes the response as the drying time changes, and the color information changes during drying. Therefore, 2 µL of sample was used in all control and test groups to prevent any interference caused by drying and to have a uniform response as well as a satisfactory color change. The *LOD* of the µPAD based on color intensity was calculated as 6.5 µM ($LOD = 3 \times \sigma$/Slope), which was higher than that of the UV–Vis absorbance-based detection due to various reasons, including heterogeneous color distribution and noise from the underlying paper structure. However, it still demonstrates the potential of the system to be trained for lower concentrations of H_2O_2. When compared to a recently published study, the system had a comparable performance with a larger detection range (Table 1). Unlike the study, the proposed system uses machine learning classifiers for a robust and adaptive H_2O_2 determination based on image features instead of color intensity data or a calibration curve, eliminating the influence of illumination variation and camera optics. The effect of pH on sensing was also tested in a pH range of 3 to 11. According to the results at 10 min, the sensor performed better at acidic and neutral pH than in basic conditions (Fig. S7).

H_2O_2 determination using machine learning

First, twenty-three classifiers were trained with images of µPADs detecting H_2O_2 at varying concentrations between 0 and 5 mM at $t = 30$ s (Fig. 4c). Based on the performance comparison, linear discriminant analysis (LDA) outperformed the others with 98.7% classification accuracy (Table S2). The same procedures were then applied for the images captured at $t = 10$ min (Fig. 4c), resulting in 98.7% classification accuracy. Note that even after 10 min, there is a small change in accuracy, proving the system stability. Maximum likelihood and Bayesian rules are used in the LDA to detect the highest likelihood between input and predefined classes based on a discriminant function that assigns units to their actual classes with minimum error [25]. The separation rules between classes are obtained with LDA in

Table 1 An overview on recently reported nanomaterial-based colorimetric methods for the determination of H_2O_2

	Detection element	Linear range (µM)	*LOD* (µM)	References
UV – Vis spectroscopy	Fe_3O_4 QDs	0.01–10,000	0.00387	[32]
	C-dots/Fe_3O_4	0.01–1000	0.001	[33]
	Hemin@CDs	0.17–33	0.11	[34]
	PtS_2 nanosheets	0.5–150	0.20	[35]
	PtS_2 @HA-DA microspheres	200–12,000	29.95	[35]
	Fe-CNNPs	0–100	0.29	[36]
	FePPOPs-SO_3H	50–1800	26.70	[37]
	Chitin-AcOH	1–900	0.052	[38]
	MnxOy/Fe_2O_3/N-doped carbon dots	0.1–2000	0.097	[39]
	Fe_3O_4@Chi	0.25–10	0.056	This work
Paper-based	Mesoporous CuO hollow sphere	10–150	2.4	[40]
	Fe_3O_4@Chi	10–500	6.5	This work

two steps. First, it is provided to find the discriminant functions that will be used to determine the real group of the trained object. Second, it is aimed to determine the group to which the object will be assigned based on the assignment rule created using these functions [26]. The robustness of the system is demonstrated by the confusion matrices shown in Fig. 6a-b. Besides classification accuracy (Eq. 1), the performance of the classifiers was also tested for precision (Eq. 2), recall (Eq. 3), and F1-score (Eq. 4).

$$\text{Accuracy} = \frac{TP + TN}{TP + TN + FP + FN} \tag{1}$$

$$\text{Precision} = \frac{TP}{TP + FN} \tag{2}$$

$$\text{Recall} = \frac{TN}{TN + FP} \tag{3}$$

$$\text{F1} - \text{score} = 2 \times \frac{\text{Precision} \times \text{Recall}}{\text{Precision} + \text{Recall}} \tag{4}$$

where FP (false positive) is the positive predictions which classified as negative by the classifier. TP (true positive) denotes the positive predictions that the classifier gives positive. TN (true negative) is the number of predictions that are classified as negative, and FN (false negative) is the number of negative predictions that the classifier could not classify as negative [27]. The most popular and simple metric to measure performance is the accuracy rate of the model that is the ratio of TP + TN to TP + TN + FP + FN. The ratio of TP to the total number of samples predicted as class positive (TP + FP) gives the precision. The recall is the ratio of TP to TP + FN. The F1-score is calculated using precision and recall metrics. Precision and recall measures alone are insufficient to draw a meaningful comparison result. Evaluation of both criteria together gives more accurate results, and the harmonic mean of precision and recall gives the F1-score [28]. The performance metrics results (Fig. 5 and Table S3) showed that LDA had the highest accuracy in terms of precision, recall, and F1-score. Classification reports and confusion matrix for $t = 10$ min are available in Table S4 and Fig. S8, respectively. At 0.5 and 5 mM H_2O_2 concentrations, the metric results are under the average values, which also seen in the confusion matrix (Fig. 6a) that visualizes the performance metrics. Briefly, one out of 28 tested samples at 0.5 mM was misclassified as 0.2 mM and two out of 28 tested samples at 5 mM were misclassified as 0.5 mM (Fig. 6a). The other concentration results were located diagonally in the confusion matrix which means that they were correctly classified. The confusion matrices show the relationship between the true and predicted classes of the classifier. In Fig. 6a-b, the true and predicted classes of

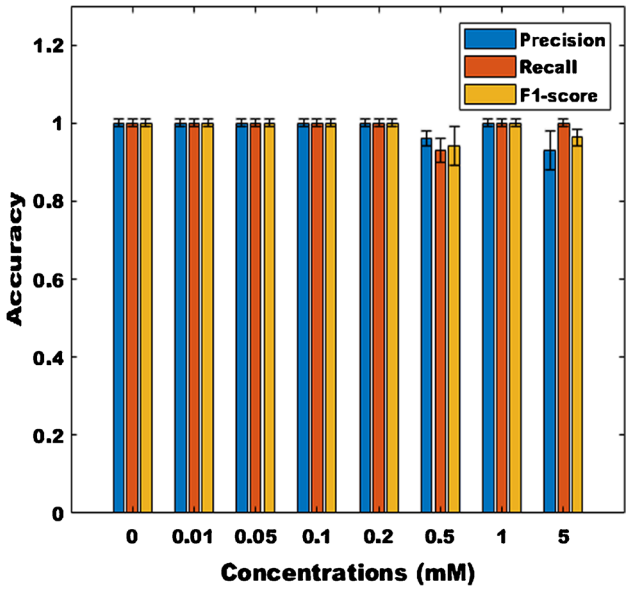

Fig. 5 The performance of LDA based on precision, recall, and F1-score at $t = 30$ s

LDA for each concentration values of H_2O_2 are shown with confusion matrices for $t = 30$ s and $t = 10$ min, respectively. Compared to the nonenzymatic platform in [12], the present system demonstrated a higher accuracy. Unlike the platform, the present system can be adopted for the detection of some biologically relevant molecules such as glucose and lactate.

Hi-perox Sens++ app and real sample analysis

The LDA classifier was integrated into a user-friendly and simple smartphone app, *Hi-perox Sens++*, for H_2O_2 detection. The app is demonstrated with the screenshots in Fig. 2 where the selected image is sent to the remote server after the crop operation. After the classification of the concentration level, the result is displayed in *Hi-perox Sens++* as in Fig. 2f, where the sample H_2O_2 was correctly classified as 1 mM. The proposed system was then tested with tap water, synthetic serum, and FBS to demonstrate its practical applicability. Synthetic serum and FBS resulted in a slightly different color than tap water. Therefore, the machine learning (ML) training dataset was expanded to include these two samples, which demonstrates the adaptability of the system to new conditions. As seen in Table S5, an acceptable recovery of H_2O_2 (104.6% for tap water, 96.9% for synthetic serum and 100.6 for FBS in average, calculated as shown in [29]) was achieved with the present system. It is worth noting that the accuracy of the system could be further boosted by training the machine learning classifier with other real samples. In addition, a selectivity test was performed with some interfering species. Real samples contain various chemicals that could potentially interfere

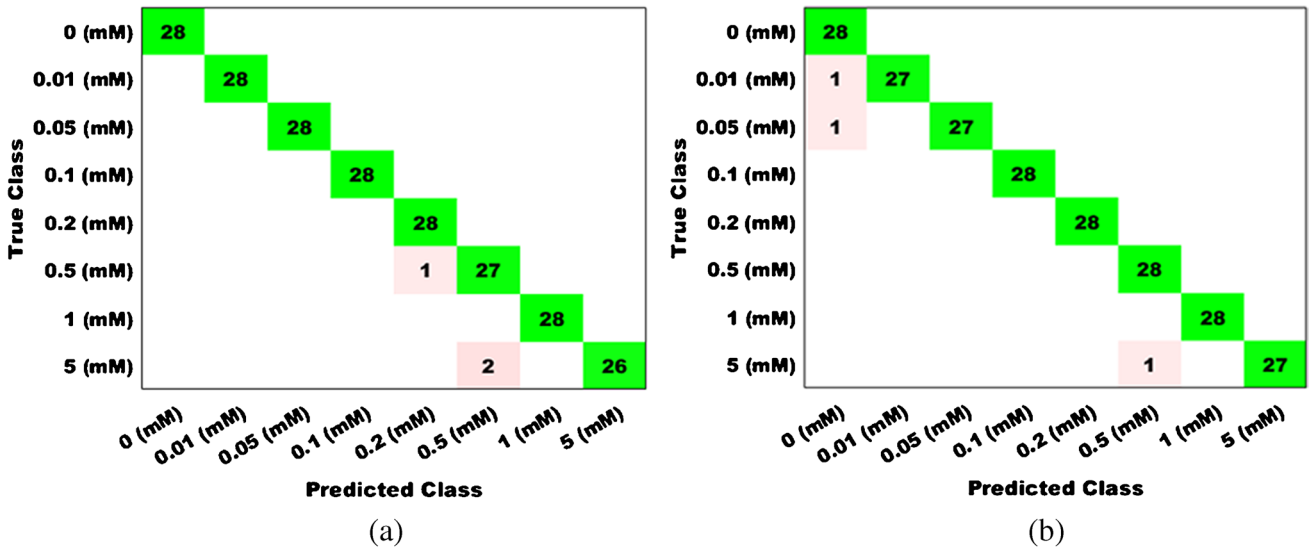

Fig. 6 Confusion matrices of Fe_3O_4@Chi NPs in varying concentrations of H_2O_2 at $t = 30$ s (**a**) and $t = 10$ min (**b**)

with the detection of H_2O_2 [30]. Therefore, various anions and cations present in tap water along with some common organic compounds were tested for the selectivity of the system. The results at 30 s clearly showed no significant difference between 0 mM H_2O_2 and 10 mM interferents (Fig. S9). However, 5 mM H_2O_2 resulted in a drastic change in the color intensity, confirming the selectivity of the sensor for H_2O_2. As the solutions in µPADs dried at 10 min, the color intensity changed proportionally in all test groups. A similar response was also observed when a mixture containing all interfering species was used as a base solution. In addition, µPADs demonstrated a relatively stable response for 8 days when they were stored in fridge (Fig. S10). It is worth noting that the µPADs were stored at + 4 °C, as TMB causes loss of sensitivity when stored at room temperature.

Although machine learning was successfully integrated to the system, it requires internet access for operation. Unlike machine learning, deep learning can be embedded into a smartphone app for off-line analysis. It also automatically extracts features for training. Therefore, deep learning will be integrated to the system in the future. Although the system is robust against illumination variation and camera optics, its robustness can be further improved by including more illumination conditions and smartphones of different brands to the training dataset. In addition, although nanozymes have the potential to overcome some of the disadvantages of natural enzymes in general, they have disadvantages such as low substrate specificity, poor biocompatibility, and potential nanotoxicity [1]. Their catalytic activity also depends on size, shape, structure, and composition. Therefore, it is possible to further improve the catalytic performance of the Fe_3O_4@Chi nanozyme by changing the synthesis conditions.

Conclusion

In this study, peroxidase mimicking Fe_3O_4@Chi nanozyme was synthesized and applied for non-enzymatic colorimetric determination of H_2O_2 using a machine learning-based smartphone app. In comparison to control group (only TMB), Fe_3O_4 NPs, and Chi, the nanozyme exhibited an excellent peroxidase-like activity and high-selectivity. Although there are many studies using nanozymes for UV–Vis-based colorimetric analysis, there are very few studies that report the use of nanozymes in µPADs and none employing artificial intelligence for colorimetric analysis. Applying nanozymes to µPADs is crucial to overcome the barrier that prevents the widespread use of these excellent materials especially in resource limited settings. To our knowledge, this is the first study to report the implementation of a machine learning-based smartphone app with a user-friendly interface for rapid and quantitative analysis of H_2O_2 in a nanozyme-based paper sensor. Machine learning provided high accuracy, phone-independent repeatability, and robustness against illumination variation and camera optics. The low *LOD* of the sensor demonstrates the potential of the system to be trained for lower concentrations of H_2O_2, which could expand the practical applications of the system. The practical applicability of the system was also demonstrated with real samples. The tested H_2O_2 concentration range might be of practical interest for applications ranging from wastewater treatment to H_2O_2 testing in food industry [31]. In sum, integrating artificial intelligence with a smartphone app makes the analysis portable, easily operable, low-cost, adaptable, and robust, which could significantly contribute to the use of such analytical tools by non-expert users.

Supplementary Information The online version contains supplementary material available at https://doi.org/10.1007/s00604-022-05474-4.

Funding This research was supported by the scientific research projects coordination unit of Izmir Katip Celebi University (Project Nos. 2021-GAP-MÜMF-0054, 2022-ÖDL-MÜMF-0007, and 2021-GAP-MÜMF-0055).

Declarations

Competing interests The authors declare no competing interests.

References

1. Ostovan A, Arabi M, Wang Y, Li J, Li B, Wang X, Chen L (2022) Greenificated molecularly imprinted materials for advanced applications. Adv Mater. https://doi.org/10.1002/adma.202203154
2. Chakraborty A, Acharya H (2021) Magnetically separable Fe_3O_4 NPs/MIL-53 (Al) nanocomposite catalyst for intrinsic OPD oxidation and colorimetric hydrogen peroxide detection. Colloids Surf A Physicochem Eng Asp 624:126830
3. Liang M, Yan X (2019) Nanozymes: from new concepts, mechanisms, and standards to applications. Acc Chem Res 52:2190–2200
4. Kilic B, Dogan V, Kilic V, Kahyaoglu LN (2022) Colorimetric food spoilage monitoring with carbon dot and UV light reinforced fish gelatin films using a smartphone application. Int J Biol Macromole 209:1562–1572
5. Guascito M, Filippo E, Malitesta C, Manno D, Serra A, Turco A (2008) A new amperometric nanostructured sensor for the analytical determination of hydrogen peroxide. Biosens Bioelectron 24:1057–1063
6. Zhang X, Bi X, Di W, Qin W (2016) A simple and sensitive $Ce(OH)CO_3/H_2O_2$/TMB reaction system for colorimetric determination of H_2O_2 and glucose. Sens Actuators B Chem 231:714–722
7. Liu Q, Zhu R, Du H, Li H, Yang Y, Jia Q, Bian B (2014) Higher catalytic activity of porphyrin functionalized Co_3O_4 nanostructures for visual and colorimetric detection of H_2O_2 and glucose. Mater Sci Eng: C 43:321–329
8. Arabi M, Ostovan A, Li J, Wang X, Zhang Z, Choo J, Chen L (2021) Molecular imprinting: green perspectives and strategies. Adv Mater 33:2100543
9. Golcez T, Kilic V, Sen M (2021) A portable smartphone-based platform with an offline image processing tool for rapid paper-based colorimetric detection of glucose in artificial saliva. Anal Sci 37:561–567
10. Arabi M, Chen L (2022) Technical challenges of molecular-imprinting-based optical sensors for environmental pollutants, Langmuir 38:5963–5967
11. Mercan ÖB (2020) Deep learning based colorimetric classification of glucose with au-ag nanoparticles using smartphone, Medical Technologies Congress (TIPTEKNO), IEEE, pp 1–4
12. Doğan V, Yüzer E, Kılıç V, Şen M (2021) Non-enzymatic colorimetric detection of hydrogen peroxide using a µPAD coupled with a machine learning-based smartphone app. Analyst 146:7336–7344
13. Mercan ÖB, Kılıç V, Şen M (2021) Machine learning-based colorimetric determination of glucose in artificial saliva with different reagents using a smartphone coupled µPAD. Sen Actuators B Chem 329:129037
14. Li G-y, Jiang Y-r, Huang K-l, Ding P, Chen J (2008) Preparation and properties of magnetic Fe_3O_4–chitosan nanoparticles. J Alloys Compd 466:451–456
15. Ragavan K, Ahmed SR, Weng X, Neethirajan S (2018) Chitosan as a peroxidase mimic: paper based sensor for the detection of hydrogen peroxide. Sens Actuators B Chem 272:8–13
16. Akyazi T, Basabe-Desmonts L, Benito-Lopez F (2018) Review on microfluidic paper-based analytical devices towards commercialisation. Anal Chim Acta 1001:1–17
17. Martinez AW, Phillips ST, Butte MJ, Whitesides GM (2007) Patterned paper as a platform for inexpensive, low-volume, portable bioassays. Angew Chem Int Ed 119:1340–1342
18. Kiliç V, Mercan ÖB, Tetik M, Kap Ö, Horzum N (2022) Non-enzymatic colorimetric glucose detection based on Au/Ag nanoparticles using smartphone and machine learning. Anal Sci 38: 347–358
19. Mercan ÖB, Doğan V, Kılıç V (2020) Time series analysis based machine learning classification for blood sugar levels, Medical Technologies Congress (TIPTEKNO), IEEE, pp 1–4
20. Srivastava M, Singh J, Yashpal M, Gupta DK, Mishra R, Tripathi S, Ojha AK (2012) Synthesis of superparamagnetic bare Fe_3O_4 nanostructures and core/shell (Fe_3O_4/alginate) nanocomposites. Carbohydr Polym 89:821–829
21. Mohammadi A, Barikani M (2014) Synthesis and characterization of superparamagnetic Fe_3O_4 nanoparticles coated with thiodiglycol. Mater Charact 90:88–93
22. Li S, Zhang T, Tang R, Qiu H, Wang C, Zhou Z (2015) Solvothermal synthesis and characterization of monodisperse superparamagnetic iron oxide nanoparticles. J Magn Magn Mater 379:226–231
23. Cao S-L, Li X-H, Lou W-Y, Zong M-H (2014) Preparation of a novel magnetic cellulose nanocrystal and its efficient use for enzyme immobilization. J Mater Chem B 2:5522–5530
24. Mucha M, Pawlak A (2002) Complex study on chitosan degradability. Polim 47:509–516
25. Fan Z, Xu Y, Zhang D (2011) Local linear discriminant analysis framework using sample neighbors. IEEE Trans Neural Netw 22:1119–1132
26. Tharwat A, Gaber T, Ibrahim A, Hassanien AE (2017) Linear discriminant analysis: A detailed tutorial. AI Commun 30:169–190
27. Chicco D, Jurman G (2020) The advantages of the Matthews correlation coefficient (MCC) over F1 score and accuracy in binary classification evaluation. BMC Genomics 21:1–13
28. Manimurugan S, Al-Mutairi S, Aborokbah MM, Chilamkurti N, Ganesan S, Patan R (2020) Effective attack detection in internet of medical things smart environment using a deep belief neural network. IEEE Access 8:77396–77404
29. Verma S, Choudhary J, Singh KP, Chandra P, Singh SP (2019) Uricase grafted nanoconducting matrix based electrochemical biosensor for ultrafast uric acid detection in human serum samples. Int J Biol Macromole 130:333–341
30. Guo X, Wang Y, Wu F, Ni Y, Kokot S (2015) A colorimetric method of analysis for trace amounts of hydrogen peroxide with the use of the nano-properties of molybdenum disulfide. Analyst 140:1119–1126
31. Riaz MA, Chen Y (2022) Electrodes and electrocatalysts for electrochemical hydrogen peroxide sensors: a review of design strategies, Nanoscale Horiz 7:463-479
32. Ahmed SR, Cirone J, Chen A (2019) Fluorescent Fe_3O_4 quantum dots for H_2O_2 detection. ACS Appl Nano Mater 2:2076–2085
33. Yousefinejad S, Rasti H, Hajebi M, Kowsari M, Sadravi S, Honarasa F (2017) Design of C-dots/Fe_3O_4 magnetic nanocomposite as an efficient new nanozyme and its application for determination of H_2O_2 in nanomolar level. Sens Actuators B Chem 247:691–696
34. Su L, Cai Y, Wang L, Dong W, Mao G, Li Y, Zhao M, Ma Y, Zhang H (2020) Hemin@carbon dot hybrid nanozymes with

peroxidase mimicking properties for dual (colorimetric and fluorometric) sensing of hydrogen peroxide, glucose and xanthine. Microchim Acta 187:1–11
35. Zhang W, Li X, Cui T, Li S, Qian Y, Yue Y, Zhong W, Xu B, Yue W (2021) PtS_2 nanosheets as a peroxidase-mimicking nanozyme for colorimetric determination of hydrogen peroxide and glucose. Microchim Acta 188:1–9
36. Xian J, Weng Y, Guo H, Li Y, Yao B, Weng W (2019) One-pot fabrication of Fe-doped carbon nitride nanoparticles as peroxidase mimetics for H_2O_2 and glucose detection. Spectrochimica Acta Part A Mole Biomol Spectrosc 215:218–224
37. Liu T, Tian J, Cui L, Liu Q, Wu L, Zhang X (2019) Facile strategy to prepare a metalloporphyrin-based hydrophilic porous organic polymer with enhanced peroxidase-like activity and high stability for colorimetric detection of H_2O_2 and glucose. Colloids Surf B Biointerfaces 178:137–145
38. Sengupta P, Pramanik K, Datta P, Sarkar P (2020) Chemically modified carbon nitride-chitin-acetic acid hybrid as a metal-free bifunctional nanozyme cascade of glucose oxidase-peroxidase for "click off" colorimetric detection of peroxide and glucose. Biosens Bioelectron 154:112072
39. Ngo Y-LT, Nguyen PL, Jana J, Choi WM, Chung JS, Hur SH (2021) Simple paper-based colorimetric and fluorescent glucose sensor using N-doped carbon dots and metal oxide hybrid structures. Anal Chim Acta 1147:187–198
40. Cheng D, Qin J, Feng Y, Wei J (2021) Synthesis of mesoporous CuO hollow sphere nanozyme for paper-based hydrogen peroxide sensor. Biosens 11:258